Wall Microstructures of High Aspect Ratio Enabled by Near-Field Electrospinning

Ahsana Sadaf, Maximilian Elter, Dario Mager, Uwe H. F. Bunz, Monsur Islam,* and Jan G. Korvink*

Near-field electrospinning (NFES) holds the potential to develop into a versatile additive nanomanufacturing platform. However, the impact of a variety of processing variables remains unresolved. Herein, the effect of solvents used to prepare suitable solutions for 3D microstructuring by electrospinning is studied. 3D straight walls of stacked fibers are fabricated using a layer-by-layer fiber deposition approach. The effect of the choice of substrate material is also explored. The results show that a high vapor pressure, and a low dielectric constant of the solvent, as well as a high substrate conductivity facilitate improved stacking of fiber layers. Utilizing these conditions, 3D stacked walls of polyethylene oxide are fabricated, and a maximum aspect ratio of 191.7 ± 52.6, while using a chromium/gold substrate and dichloromethane/methanol as the solvent is achieved.

1. Introduction

Additive micromanufacturing refers to the fabrication of microstructural building blocks and their assembly into higher order.[1–3] The structures obtained from additive micromanufacturing can exhibit surprisingly rich and programmable properties, which can have a significant impact in various fields ranging from energy devices[4,5] to biomedical applications.[6–9] The properties of the final products strongly depend on the constituent material, and the control of the microstructural material in 1D, 2D, and 3D, which further depends on the resolution, processing speed, and material processing.[2] To date, lithography-based technologies, such as e-beam lithography,

nano-imprint lithography, and direct laser writing, have enabled additive nanomanufacturing with a resolution down to tens of nanometers and with high controllability at this scale.[10,11] However, these methods feature major drawbacks, including extremely slow processing speed, and the use of expensive and sophisticated infrastructure, which bar these technologies from scaling up easily. Furthermore, the materials used in these methods are predominantly limited to epoxy-based photoresists. Therefore, there is a critical need for technologies that can enable additive nanomanufacturing of materials beyond photoresists, with a high processing speed and high resolution, toward scalable and rapid fabrication of 3D structures with programmable properties. NFES is a promising technique, which has the potential to satisfy these requirements, if its limitations can be overcome.

NFES is a method of patterning nanofibers utilizing the strong interaction of a charged polymer droplet in an electric field with a short distance to the substrate.[12,13] It features several advantages over other patterning technologies. It can achieve nanofiber patterning with a resolution down to tens of nanometers, with a high printing speed ($>20 \, cm \, s^{-1}$), and high precision of nanofibril deposition.[14,15] A variety of materials beyond polymers can be thus patterned, which includes carbon, metal oxides, and composites.[16–20] Despite these advantages, NFES has been mostly constrained to the patterning of planar geometries. Due to its high printing speed and control of nanofibril deposition, it, however, holds a strong potential towards evolving into a high-speed additive nanomanufacturing tool. Toward this goal, several researchers have recently focused on this endeavor. Park et al. demonstrated the fabrication of different shapes of 3D walls with an aspect ratio ranging from 48 to 72. The authors reported the enhancing of charge dissipation of the deposited fibers, and tuning the conductivity of the electrospinning solution through the addition of sodium chloride (NaCl) into the polymer solution.[21] Luo et al. reported the fabrication of different 3D structures of electrospun fibers while using printing paper as a collector.[22] The porous nature of the collector paper provided a rigid supporting base for the initial layers of the electrospun fibers, which facilitated the subsequent layer-by-layer fibril deposition. Zheng et al. reported that layer-by-layer 3D nanofibril construction was achieved by a sharp-tip guiding electrode.[23] In their report, the tip electrode was placed behind the

A. Sadaf, D. Mager, M. Islam, J. G. Korvink
Institute of Microstructure Technology
Karlsruhe Institute of Technology
Hermann-von-Helmholtz-Platz 1
76344 Eggenstein-Leopoldshafen, Germany
E-mail: monsur.islam@kit.edu; jan.korvink@kit.edu

M. Elter, U. H. F. Bunz
Institute for Organic Chemistry
Ruprecht-Ksarls-Universität Heidelberg
Im Neuenheimer Feld 270, 69120 Heidelberg, Germany

The ORCID identification number(s) for the author(s) of this article can be found under https://doi.org/10.1002/adem.202101740.

**ADVANCED
SCIENCE NEWS**

www.advancedsciencenews.com

**ADVANCED
ENGINEERING
MATERIALS**

www.aem-journal.com

collector, which guided the precise deposition of the nanofibers on the collector by enhancing the charge transfer process and weakening the electrical interference. This process resulted in 3D structures with an aspect ratio as high as 25. It should be pointed out here that to facilitate the 3D structuring using NFES, all these existent reports used additional modifications to the primitive NFES set up either in terms of auxiliary guiding electrode, use of porous collector for rigid support, or tuning the conductivity by modifying the polymer solution. Even though they resulted in successful 3D structuring, these modifications can cause additional sophistication to the system and the resulting materials, which might increase complexity in the usability of the system, or restrict the use of the fabricated structures in many applications. We believe that 3D structuring of electrospun fibers can be also possible using a traditional NFES system, solely by studying different fundamental process parameters of NFES for layer-by-layer stacking of electrospun fibers. Extensive study of different process parameters will elucidate the mechanism of 3D structuring, which can be further tuned for any specific applications.

Our work thus aims to study different processing variables in the 3D structuring of microfibers using NFES. We particularly studied the effect of the properties of the solvent, substrate properties, and collector speed in fabricating 3D walls of stacked microfibers through the layer-by-layer deposition of electrospun microfibers. Based on the results obtained here, we postulate a mechanism for microfiber stacking. This study thus represents a first step towards the fabrication of complex 3D architectures of microfibers.

2. Results and Discussion

The experimental procedure used in this work is schematically presented in **Figure 1**. We chose polyethylene oxide (PEO) as the electrospinnable polymer feedstock due to its high popularity in NFES.[24] In NFES, the dominant factors of a solvent are conductivity, dielectric constant, and vapor pressure.[25,26] To investigate

Table 1. Properties of solvents used to prepare the PEO solutions for electrospining.

Solvent	Conductivity [mS m^{-1}]	Dielectric constant	Vapor pressure [kPa]	References
Water	0.447	78.4	3.16	[38,39]
Methanol	0.1207	32.6	13.02	[38,40]
Dichloromethane	0.505	8.93	53.3	[38,41]

a wide range of these properties in the 3D stacking of electrospun fibers, we chose de-ionized water, methanol, and dichloromethane (DCM) as the solvents for solution preparation. The properties of these solvents are listed in **Table 1**. Unmodified silicon wafers, silicon oxide coated silicon wafers (SiO2/Si), and chromium and gold (Cr/Au) coated silicon wafers were used as the substrate material to explore the effect of substrate conductivity on electrospun fibril stacking. In our NFES setup, we used a rotating drum (diameter = 14 cm) as the collector, as we only focused on the fabrication of 3D stacked walls by exploring the stacking behavior. Continuous rotation of the drum collector was expected to facilitate layer-by-layer fiber deposition, as the spinneret was kept stationary, and the shorter distance between spinneret and collector minimized the fiber deflection.

We started our stacking experiments using an aqueous solution of PEO. Upon electrospinning, the aqueous solution resulted in a heap-like structure of stacked fibers (Figure S1, Supporting Information), irrespective of the choice of the substrate material. Such behavior can be attributed to the high dielectric constant and the low vapor pressure of water. The high dielectric constant of water ($\varepsilon_r = 78.4$) led to a high surface charge retention within the deposited fibers. The excess surface charge of the deposited fibers exerts a repulsive force on the upcoming fiber stream, competing with the force due to fiber tension, yielding an offset in the positioning of the upcoming fiber. Furthermore, the low vapor pressure of water led to incomplete evaporation during electrospinning, resulting in
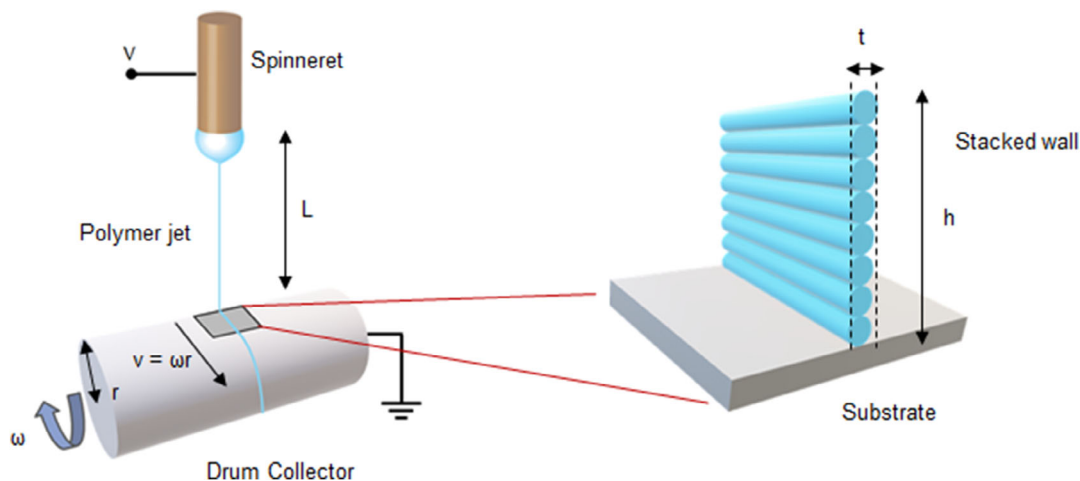

Figure 1. Schematic of the near-field electrospinning (NFES) setup showing the layer-by-layer deposition of fibers towards the fabrication of 3D stacked walls. The characteristic parameters of the system are indicated in the schematic, which are the distance between spinneret and collector (L), drum radius (r), and rotational speed of drum (ω). The surface velocity (v) is defined as $v = \omega r$. h is the height of the stacked wall and t is the thickness of the wall.

the retention of excess water within the deposited fiber. The residual water led to the merging of the partially overlapped fiber layers, resulting in the experimentally observed heap-like structures.

The introduction of methanol within the aqueous solution minimized the fibril layer offsets, leading to the successful stacking of the fibers. This improvement was attributed to the lower dielectric constant of methanol ($\varepsilon_r = 32.6$) than that of water. A lower dielectric constant results in a lower number of charge carriers within the solvent.[27] Therefore, it was plausible that the addition of methanol to the solvent system led to a reduced number of residual charge carriers within the polymer solution. Furthermore, methanol features a higher vapor pressure than water (see Table 1), which led to faster evaporation of the solvent for the binary solvent system. Faster evaporation during electrospinning jetting resulted in minimal solvent retention within the deposited fiber. These phenomena synergically decreased the amount of surface charge of the electrospun fibers, minimizing the repulsive force between deposited and arriving fibers, and improving the positioning of the fiber deposition process.

Even though the addition of methanol facilitated stacking of the electrospun fibers, the choice of the substrate and the concentration of methanol exhibited a strong influence on the stacking behavior. **Figure** 2A,B shows the effect of these two parameters on the height and diameter of the stacked walls, respectively, when the number of drum rotations was kept constant at 20 and the linear substrate speed was $100\,\mathrm{cm\,s^{-1}}$. We focused on achieving a stacked wall with a high aspect ratio

(=height/diameter). Therefore, stacked walls featuring an enhanced height and a reduced diameter were desired. Among the three substrates used in this work, Cr/Au substrate resulted in the tallest height and smallest diameter, irrespective of the concentration of methanol in the solution, as shown in Figure 2A,B. The SiO2/Si substrate exhibited the poorest dimensions. The Cr/Au substrate featured the highest conductivity due to its metallic nature, whereas the SiO2/Si substrate had the lowest conductivity due to the insulating coating of SiO2. The Si substrate is of a semiconducting nature, having a conductivity higher than the SiO2/Si substrate and lower than the Cr/Au substrate. This is in agreement with a previous report by Park et al., where they suggested that a conductive surface facilitates faster charge dissipation from the deposited fibers lowering their accumulated surface charges.[21] Faster charge dissipation from the deposited fibers minimized the repulsive force between the already deposited fiber and the next fibers, which facilitated the deposition of the upcoming stream with a minimal offset leading to better stacking.

The effect of the substrate can be further visualized in the morphology and shape of the stacked walls. Figure 2D–F shows the scanning electron microscope (SEM) images of the stacked walls on the SiO2/Si, Si, and Cr/Au substrates. The stacked wall on the SiO2/Si substrate appeared as a large heap-like structure, which was due to the poor stacking of the fibers. The insulating behavior of the SiO2 coating yielded a poor charge dissipation of the residual charges within the deposited fibers. As mentioned earlier, the residual charge residing on the fibers had a great impact on the positioning of fibers. The fibers that were
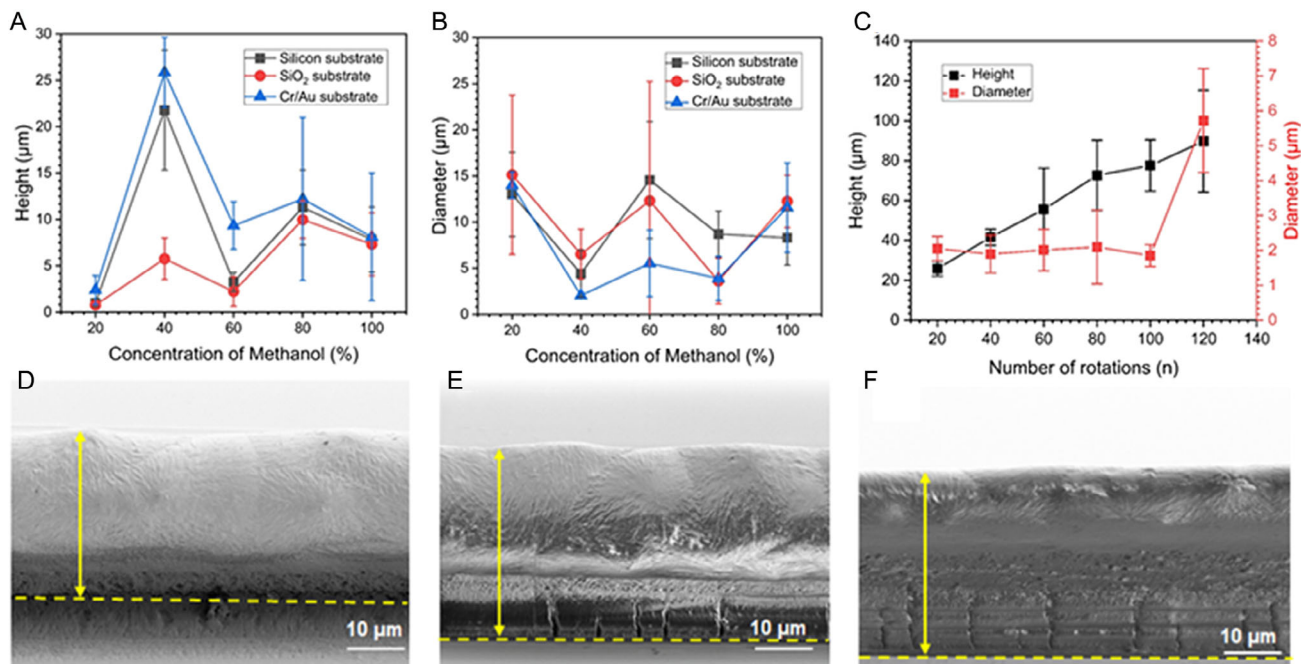

Figure 2. The effect of the concentration of methanol on the: A) wall height and B) polyethylene oxide (PEO) fiber diameter using a water/methanol solvent system and different substrates (SiO$_2$, Silicon, Cr/Au). The fiber diameter was measured at the top layer. The number of drum rotations was set to 20. C) The effect of the number of drum rotations on the dimensions of stacked fibers while using 40% methanol/60% water on Cr/Au substrate. Scanning electron microscope (SEM) images of the stacked fibers using 40% methanol/60% water on: D) SiO2/Si, E) Silicon, and F) Cr/Au substrates. The SEM was performed by tilting the SEM stage by 65°. The dashed lines in (D), (E), and (F) represent the interface between the substrate and the stacked wall, and the double arrow indicates the height of the stacked wall. The drum speed used for these experiments was $100\,\mathrm{cm\,s^{-1}}$.

**ADVANCED
SCIENCE NEWS**

www.advancedsciencenews.com

**ADVANCED
ENGINEERING
MATERIALS**

www.aem-journal.com

supposed to stack on each other, dislocated and landed next to the pre-deposited fibers, due to repulsion by the residual charge on fibers. Further deposition might have taken place at closer proximity, overlapping with the pre-deposited fibers. Furthermore, the deposited fibers might still have retained some of the solvents, due to incomplete evaporation of the solvents within the shorter distance used in NFES. In comparison to the SiO2/Si substrate, the stacked wall on the Si and Cr/Au substrates exhibited straighter features, evidenced by the rounded top feature of the stacked wall, which was smaller, with the smallest radius for the Cr/Au substrate. However, no individual layer was observed within the stacked walls, irrespective of the choice of substrate. The walls featured a porous microstructure, which can be attributed to phase separation of the solvent during the drying process.[28] For a polymer solution prepared using a binary solvent, liquid–liquid demixing can occur, in which the solution is separated into a polymer-rich and a polymer-lean phase.[29] In our solution, PEO was more readily soluble in water than methanol,[30] yielding PEO-water as the polymer-rich phase and PEO-methanol as the polymer-lean phase. Due to a stronger interaction of the polymer-rich phase, water became the primary solvent in our solution. During the drying process, methanol triggered the phase-separation, leaving a porous microstructure upon drying.[31] The higher vapor pressure of methanol compared to water (Table 1) further led to faster evaporation of the methanol, intensifying the phase separation. Furthermore, the effect of the phase separation seemed to be more drastic when comparing the top to the bottom of the stacked wall, as more porous features were observed toward the base of the wall, as shown in the high magnification SEM images of different spots of the wall fabricated on the Cr/Au substrate (Figure 2B,C, Supporting Information). Particularly, several cracks were observed at the base of the wall, as shown in Figure 2D, Supporting Information, which might have resulted due to the interaction between the substrate and the deposited fibers. As mentioned earlier, rapid layer-by-layer deposition of the electrospun fibers restricted complete evaporation of the excess residual solvent from the layers of the stacked walls.

This became severe toward the base region. Residual water might have accumulated toward the base, as further layers got deposited, due to a gravitational effect, and phase separation by the methanol. The accumulated water evaporated slowly due to its low vapor pressure. The high surface tension of the water further led to the generation of high internal stress within the base layers of the stacked wall, resulting in the formation of cracks. However, no cracks were observed within stacked fibers that got detached from the substrate at the edge of the substrate, as shown in Figure S3, Supporting Information. It might be that the evaporation and phase separation occurred uniformly, as there was no gravitational effect and no substrate interaction. Due to such a uniform drying process, separate fibril layers could be also seen for the free-standing stacked walls. As a conductive substrate yielded better stacking, we performed further experiments only using Cr/Au substrates.

Figure 2A,B also shows the effect of methanol concentration on the dimensions of the stacked walls. 20% methanol concentration exhibited the poorest result among the binary solvent systems, featuring the lowest height and broadest diameter. Even though stacking was achieved with 20% methanol, the water present within the system overpowered that of methanol. Hence, the quality of stacking improved significantly as the methanol proportion increased within the binary solvent. At a proportion of 40% methanol, the best stacking results were obtained, featuring the tallest stack height of $25.9 \pm 3.8\,\mu m$, and the narrowest diameter of $2.1 \pm 0.4\,\mu m$. We hypothesize that the PEO solution featuring 40% methanol achieved a critical ionic concentration within the polymer-solvent system, facilitating a sufficient number of charge carriers to travel to the collector, with minimal remaining surface charge in the deposited fiber, and minimal residual solvent that facilitates dissipating the surface charge effectively. Expectedly, the 40% methanol mixture also achieved the highest aspect ratio among all the concentrations, as shown in **Figure 3**A. A further increase in the methanol concentration resulted in poorer results in terms of the dimensions of the stacked walls (Figure 2A,B, and 3A). An increased methanol concentration enhanced the overall number
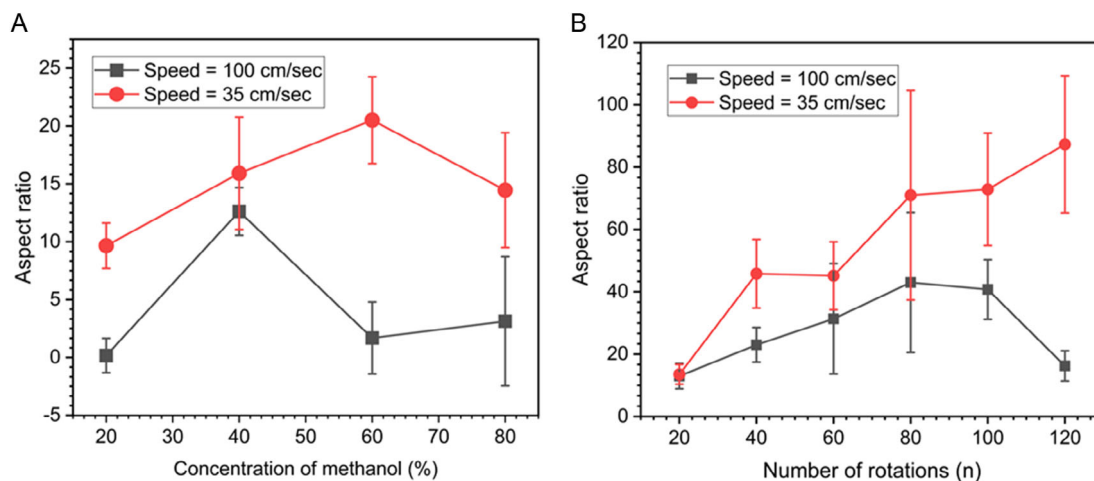

Figure 3. Effect of drum speed on the aspect ratio of stacked walls of PEO while using a water/methanol binary solvent system for different: A) concentration of methanol and B) number of drum rotations. The number of drum rotations for the data in (A) was 20. The PEO solution with 40% methanol was used for the experiments presented in (B). Cr/Au substrates were used for all the experiments.

of charge carriers, which might have resulted in a slower charge dissipation and led to poor stacking.

The number of rotations of the drum collector significantly impacted the dimensions of the stacked walls. As expected, taller walls were achieved with an increased number of rotations, as shown in Figure 2C. The height of the stacked wall increased linearly from $25.9 \pm 3.8 \mu m$ for 20 rotations to $89.7 \pm 25.5 \mu m$ for 120 rotations. Interestingly, the diameter of the top layer of a stacked wall did not vary significantly up to 100 rotations; the diameter remained within a range 1–2 μm. For 120 rotations, the wall diameter increased to $\approx 6 \mu m$. This behavior could be due to the saturation of evaporation of the solvent in the structure. The layers deposited after 100 rotations might have fused into each other due to inadequate solvent evaporation, resulting in the broadening of the top layer. We further plotted the aspect ratio for different numbers of rotations for 40% methanol in Figure 3B. The aspect ratio increased from 13 ± 4.1 for 20 rotations to 43 ± 22.4 for 80 rotations, and afterward decreased to 16.2 ± 4.8 for 120 rotations. The low aspect ratio for 120 rotations was only a consequence of the broadening of the top layer of the stacked wall.

We further studied the effect of drum speed on the geometrical features of the stacked walls by performing additional experiments with a drum speed of $35 \, \text{cm s}^{-1}$. Surprisingly, a lower drum speed resulted in a better stacking performance, both while varying the methanol concentration, and the number of rotations, as shown in Figure 3A,B, respectively. For example, the highest aspect ratio achieved for a drum speed of $100 \, \text{cm s}^{-1}$ was 43 ± 22.4, whereas a drum speed of $35 \, \text{cm s}^{-1}$ yielded the highest aspect ratio of 80 ± 20.3. Furthermore, the aspect ratio for a drum speed $35 \, \text{cm s}^{-1}$ increased linearly with the number of drum rotations, as shown in Figure 3B. This should be expected, as the height of the stacked walls increased linearly with the number of fibre layers, whereas the diameter remained almost unchanged (Figure S8, Supporting Information). Figure 4A–D show SEM images of stacked walls at an increasing number of drum rotations, emphasizing the increasing height of the stacked walls. The stacking behavior also seemed to improve as the number of rotations increased. For example, 20 rotations led to the formation of fused layers of fibers, leaving a highly porous broad bottom layer (Figure 4A). As the number of rotations increased, the walls became straighter and less porous. Even individual layers of deposited fibers could be observed within the stacked walls (Figure 4B–D), which was unlikely to be the case for the speed of $100 \, \text{cm s}^{-1}$ (Figure 2F). However, several cracks appeared along the stacked walls due to the phase-separation-induced stress within the deposited layers. Nevertheless, we speculate that the improvement in stacking with lower drum speed could be attributed to the slower fiber deposition rate arising from the slower drum speed itself. A slower deposition rate might have provided enough time to the already deposited layer to dissipate the residual surface charges into the conductive substrate before the arrival of the subsequent layer, yielding a better stacking. Furthermore, a slower deposition rate also provided sufficient time for evaporation of the residual solvent from the already deposited fibers,
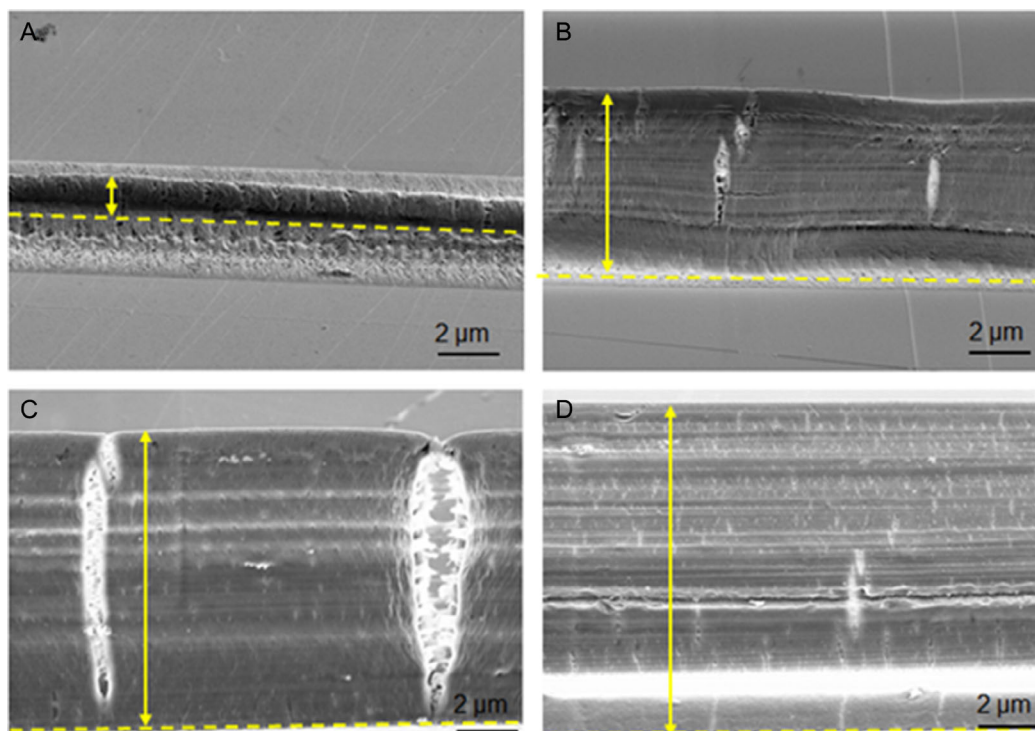

Figure 4. SEM images of the stacked fibers of PEO with the number of drum rotations of: A) 20, B) 60, C) 100, and D) 120. The PEO solution with methanol (40%)/water (60%) binary solvent and the drum speed of $35 \, \text{cm s}^{-1}$ were used for the experiments. The stacking was performed on Cr/Au substrates. SEM was performed by tilting the SEM stage by 65°. The dashed lines represent the interface between the substrate and the stacked wall, whereas the double arrow indicates the height of the stacked wall.

which led to the formation and retention of individual layers. It should be noted here that, for a speed of 35 cm s^{-1}, best stacking results were obtained for the methanol concentration of 60%, whereas 40% methanol exhibited the best stacking behavior for the drum speed of 100 cm s^{-1}. We are not sure about the correlation between drum speed and optimal methanol concentration. Due to a limitation of our experimental setup, we could not perform experiments with intermediate drum speeds. Further experiments are needed with intermediate speeds to fully elucidate the effect of speed and its correlation with solvent concentration, to find an optimal rate. As a drum speed of 35 cm s^{-1} exhibited better stacking in our experiments, we performed our further experiments using the same speed.

Overall, experiments with the water/methanol solvent system suggested that faster evaporation led to better stacking. To achieve a faster evaporation during stacking, we investigated the use of DCM as a solvent. DCM features a vapor pressure of 53.3 kPa, which is significantly higher than water and methanol. We also used the drum speed of 35 cm s^{-1} here, as the slower speed facilitated better evaporation of residual solvent during layer-by-layer deposition. Furthermore, it also features a low dielectric constant (8.93), which is beneficial for stacking,

due to the lower amount of retained charges that need to be dissipated. Methanol proved to be a good choice of solvent to enhance stacking, due to its comparatively higher vapor pressure and lower dielectric constant than water. Therefore, we replaced water with DCM in the binary solvent system, and studied the effect of different concentrations of DCM on the stacking behavior.

As we had speculated, DCM/methanol binary system facilitated successful stacking. Like the water/methanol system, the dimensions of the stacked walls also depended on the solvent proportionality and the number of drum rotations. As expected, taller walls were achieved with an increased number of rotations (**Figure** 5A), whereas diameter did not vary significantly (range: $1.3 - 2.1\mu$m, see Figure S7, Supporting Information). Therefore, the aspect ratio also increased linearly with the number of rotations (Figure 5B). The height and aspect ratio of the stacked walls also exhibited an increasing trend with an increase in DCM concentration, as shown in Figure 5A,B. We achieved continuous fiber deposition for the maximum DCM concentration of 60%. A concentration above 60% DCM tended to dry up at the spinneret due to rapid evaporation, disrupting continuous fiber deposition, therefore causing trouble during fibril stacking.
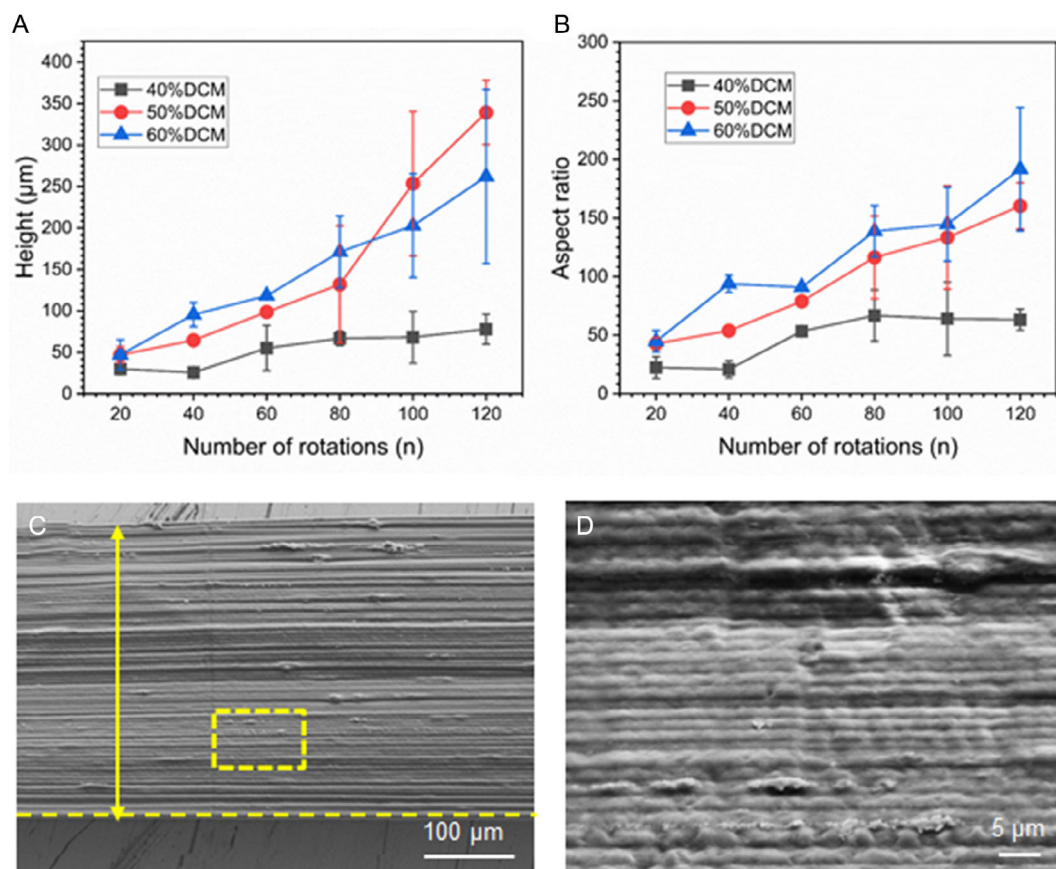

Figure 5. The effect of dichloromethane (DCM) concentration on: A) the height and B) aspect ratio of a stacked wall of PEO fiber, while using the DCM/methanol binary solvent system for different numbers of rotations. C) SEM image of the stacked wall of the PEO solution with methanol (40%)/DCM (60%) binary solvent and a drum speed of 35 cm s^{-1} was used for all the experiments. The number of rotations for the fabricated wall shown in (C) was 100. D) High magnification image of the rectangular section shown in (C), emphasizing the layer-by-layer deposition of electrospun fibers. SEM was performed by tilting the SEM stage by 65°. The dashed line and the double arrow line in (C) represent the interface between the substrate and the stacked wall and the height of the stacked wall, respectively. Cr/Au substrates were used for the experiments.

Faster evaporation of DCM led to a stacked wall with many superior dimensional features compared to the water/methanol system. The highest aspect ratio achieved for the water (60%)/methanol (40%) system was 80 ± 20.3, whereas the DCM (60%)/methanol (40%) system yielded a remarkable highest aspect ratio of 191.7 ± 52.6. This is, to the best of our knowledge, the highest aspect ratio reported for any fabricated structure achieved by electrohydrodynamic 3D printing. For comparison, the highest aspect ratio achieved by X-Ray LIGA technology lies in the range of 100–200,[32] and is still considered the record holder. Even though DCM facilitated the formation of such high aspect ratio walls, these walls tended to fall under their own weight, or through system-generated vibrations due to their fragility. Our ongoing efforts are focusing on the stabilization of these high-aspect ratio structures.

Along with the dimensional features of the stacked wall, DCM also led to cleaner microstructures of the walls. Figure 5C,D shows low and high magnification SEM images of the stacked wall of PEO obtained from the DCM/methanol system. Distinct layers of the stacked walls are visible, which resemble the layer arrangements of any typical additive manufacturing technique. The morphology of the wall still featured a porous microstructure, which was expected due to the rapid evaporation of the solvent. However, the porosity of the walls seemed significantly less severe compared to the walls obtained for the water/methanol solvent system. This also suggested the accumulation of minimal residual solvent within the electrospun fiber layers for the DCM/methanol system, thanks to the high vapor pressure of DCM. It should be noted that, over time, the structures fabricated using DCM developed numerous cracks along and perpendicular to the layers. We speculate that the rapid evaporation of the DCM might have resulted in significant internal stress within the stacked layers, which were released over time. The relaxation process might have initiated the cracks, which propagated gradually (Figure S6A,B, Supporting Information). The relaxation process further caused other structural deformities, including curling, curving, and inclining of the stacked walls. The inclination effect can be observed for taller structures (120 rotations), as evidenced by an SEM image of the stacked wall (Figure S5B, Supporting Information). However, the straight part of the stacked wall can be observed in Figure S5C, Supporting Information, showing a high aspect ratio.

We propose here a mechanism for 3D stacking of electrospun fibers based on the results obtained in this study and the information available in the literature regarding NFES. The mechanism involves three major aspects: 1) straight trajectory of polymer jet; 2) evaporation of the solvent; and 3) charge dissipation upon deposition (**Figure 6**). Even though we did not study the trajectory of polymer jet in this work, it is important to discuss here, as the straight trajectory ensures precise deposition of the fibers. At the initiation, similar to classical electrospinning, a polymer jet is ejected from the Taylor cone of the polymer droplet when the applied electric field reaches a threshold value. The small distance between spinneret and collector in NFES restricts the jet deflection. However, a fair competition between viscoelastic force (F_v) and between electrostatic repulsive force (F_r) on the ejecting jet determines the straightness of the jet trajectory.[33] F_v originating from the long-chain entanglement within the polymer solution works in the favor of straight trajectory, whereas F_r arising from surface charge attempts for jet deflection. Several parameters, including applied voltage, spinneret
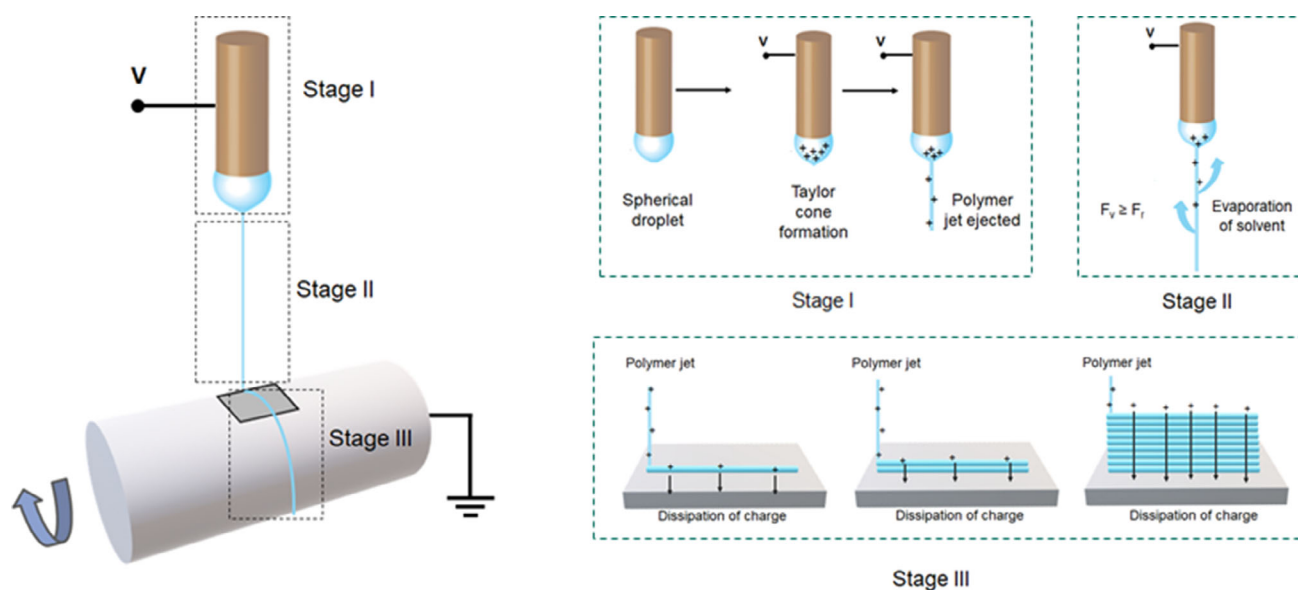

Figure 6. Schematic showing the proposed mechanism of layer by layer deposition of fibers toward the fabrication of 3D stacked structures. The leftmost image shows the NFES setup comprised of three stages. Stage I shows the formation of the Taylor cone upon applying high voltage. After reaching a threshold value, the polymer jet is ejected. In stage II, the jet traveled in a straight path as viscoelastic forces (F_v) are greater than repulsive forces (F_r) maintaining the linearity of the jet. As the jet is stretched, the solvent evaporates. In stage III, as the fiber reaches the collector, the residual charge on the fiber dissipates into the collector, attracting the jet towards the already deposited fiber, forming a 3D stacked wall.

to collector distance, and viscosity and conductivity of polymer solution play crucial roles in determining the balance of these two forces. Nevertheless, a dominating F_v is desired for achieving precise fiber deposition, leading to 3D stacking. A solution with a high viscosity is preferred in this context. During the flight of the jet, the solvent present within the polymer jet evaporates and the surface charge dissipates in the surrounding air. Complete evaporation of the solvent is expected before the deposition of the fiber on a collector. Therefore, a solvent system with a high vapor pressure is expected for fast evaporation. However, the deposited fibers retain excess solvent due to the short spinneret-to-collector distance used in NFES. The residual solvent further increases the number of free surface charges on the already deposited fibers. Accumulation of the residual surface charges on the deposited fibers can cause a repulsion force to the incoming fibers. It can result in a deviation of the path of the incoming fiber, which can cause the stacking to fail. Therefore, a fast dissipation of the residual surface charge is essential for the stacking of the fibers. The high conductivity of the collector facilitates fast charge dissipation due to its fast electron transfer characteristic. The fast charge dissipation and the straight trajectory of the polymer jet allow subsequent fibers to deposit upon each other, forming the 3D wall. It should be noted that the proposed mechanism is based on the process parameters studied here, i.e., solvent properties, collector conductivity, and collector speed. Other fundamental parameters need to be studied extensively for 3D stacking on electrospun fibers, which may further elucidate the complete mechanism. Furthermore, the current study raises additional questions on the behavior of binary solutions in NFES. We only used three solvents here, which are not enough to fully understand the solvent effect. As the focus here was to investigate the manufacturability of 3D structures using NFES, the characterization study of binary solvents was out of the scope of this communication. A detailed study on binary solution systems (or more) involving a variety of solvents needs to be conducted to characterize their properties relevant to electrospinning and their impact on 3D structuring.

3. Concluding Remarks

In summary, we achieved the fabrication of 3D walls through the layer-by-layer stacking of near-field electrospun fibers on a drum collector. Solvent properties, such as dielectric constant and vapor pressure, collector speed, and substrate conductivity played a crucial role in the stacking behavior of electrospun fibers. A low dielectric constant translated to a low surface charge retention upon deposition, which allowed the upcoming fibers to deposit onto previously deposited fibers, yielding more precise stacking. Furthermore, a higher vapor pressure of the solvent enhanced the stacking behavior due to its fast evaporation. Additionally, a binary solvent system exhibited better stacking results compared to a single solvent system, as the binary system allowed to tune the conditions preferable for stacking. By tailoring these properties, we fabricated 3D stacked walls of PEO and reached a maximum aspect ratio of 191.7 ± 52.6, while using a chromium/gold substrate and DCM/methanol as the binary solvent. Even though we focused our experiments only on the fabrication of

3D walls, the current results are promising. It suggests that, in controlling the fundamental parameters of NFES, the process could lead to structures of remarkably high aspect ratio geometrical features. As it is mentioned earlier other parameters, for example, properties of polymer, geometry of spinneret, collector geometry, and surrounding environment, may have a substantial impact on the stacking mechanism and the morphology of the stacked wall, which needs to be investigated extensively. For instance, coaxial spinneret leads to the formation of core–shell fibers.[34] Utilizing coaxial spinneret for stacking experiments can lead to the fabrication of multi-material 3D walls, which may perform enhanced structural stability. Additionally, judicious choice of core-shell solutions can also lead to 3D walls of hollow fibers,[35] resulting in high surface-area hierarchical structures, which can exhibit superior results in applications, such as drug delivery, heat-sink, and filtration. Furthermore, with a judicious choice of polymer solution combined with an additional post-processing step, this process could facilitate the additive nanomanufacturing of material structures beyond photo-polymers, including carbon, ceramics, and composites of hard materials. For example, 3D stacking of a carbonizable polymer followed by a carbonization step can be a facile pathway for fabricating 3D carbon microelectrodes, alternative to the photolithography-based fabrication route primarily used in carbon microelectromechanical system (C-MEMS) technology.[36,37] Even though the current study only used a rotating drum as a collector, replacing the drum with a high-speed X-Y stage will add more design freedom for the fabrication process, as it will allow high-speed fabrication of complex structures generated from a computer-aided design. This will be a step forward toward the scaling-up process of NFES-assisted additive micro/nano-manufacturing technology.

4. Experimental Section

Solution Preparation: PEO was used, featuring a molecular weight of 300 000 (Alfa Aesar, LOT: Z22C004) as the electrospinnable polymer feedstock. De-ionized water, methanol, and DCM were used as solvents. The electrospinnable solution was prepared by adding PEO (10%wt) in the solvent, followed by stirring at 1000 rpm for 12 h at room temperature.

NFES: The electrospinning solution was placed in a horizontally fixed syringe (1 mL) equipped with a stainless steel needle with an inner diameter of 250 μm. The solution was electrospun using a custom-built NFES setup, consisting of a DC voltage power supply (Heinzinger, PNChp 6000), a syringe pump (Chemyx FusionTouch 100-X), and a custom-built and grounded rotating drum collector. Three different kinds of substrate were used in the work: unmodified silicon wafers (N-doped, thickness $525 \pm 25\mu$m, conductivity 0.1–1 S cm^{-1}), silicon wafers coated with an oxide layer (1μm), and chromium (10 nm) and gold (60 nm) coated silicon. Two different rotating drum systems were used in the work. Both systems featured drums with a diameter of 14 cm, but enabled different linear speeds of the substrate with respect to. the spinneret: 35, or 100 cm s^{-1}. The distance between the spinneret and the grounded drum collector was kept in the range of $1-2$ mm. A voltage in the range of $900-1000$ V was applied to the needle during the electrospinning process.

Characterization: The electrospun fibril layers were observed using an optical microscope (VHX-100K Series Digital Microscope), immediately after the deposition to facilitate fast screening of the manufacturing process. The fabricated structures were further investigated using scanning electron microscope (Carl Zeiss AG—SUPRA 60VP SEM) for detailed morphological characterization. The height of the stacked fibers was measured using a chromatic white light interferometer (Bruker Contour GT-K).

The diameter of the fabricated structures was measured at the top layer of the structure, which was not subject to squeezing effects from above.

Supporting Information

Supporting Information is available from the Wiley Online Library or from the author.

Conflict of Interest

The authors declare no conflict of interest.

Data Availability Statement

The data that support the findings of this study are available from the corresponding author upon reasonable request.

[1] K. P. Cooper, *Micro-and Nanotechnology Sensors, Systems, and Applications XI*, Vol. *10982*, International Society for Optics and Photonics, Bellingham, WA **2019**, p. 1098213.

[2] D. S. Engstrom, B. Porter, M. Pacios, H. Bhaskaran, *J. Mater. Res.* **2014**, *29*, 1792.

[3] I. Liashenko, J. Rosell-Llompart, A. Cabot, *Nat. Commun.* **2020**, *11*, 1.

[4] G. Zheng, W. Li, X. Wang, H. Wang, D. Sun, L. Lin, in *2010 IEEE 5th Inter. Conf. on Nano/Micro Engineered and Molecular Systems*, IEEE, Piscataway, NJ **2010**, pp. 284–288.

[5] S. W. Choi, S. M. Jo, W. S. Lee, Y.-R. Kim, *Adv. Mater.* **2003**, *15*, 2027.

[6] D. Liang, B. S. Hsiao, B. Chu, *Adv. Drug Delivery Rev.* **2007**, *59*, 1392.

[7] X. Mo, C. Xu, M. Kotaki, S. Ramakrishna, *Biomaterials* **2004**, *25*, 1883.

[8] H.-J. Jin, J. Chen, V. Karageorgiou, G. H. Altman, D. L. Kaplan, *Biomaterials* **2004**, *25*, 1039.

[9] M. Islam, A. D. Lantada, D. Mager, J. G. Korvink, *Adv. Healthcare Mater.* **2021**, 2101834.

[10] K. Malladi, C. Wang, M. Madou, *Carbon* **2006**, *44*, 2602.

[11] H. Jiang, S. I. Stupp, *Langmuir* **2005**, *21*, 5242.

[12] D. Sun, C. Chang, S. Li, L. Lin, *Nano Lett.* **2006**, *6*, 839.

[13] X.-X. He, J. Zheng, G.-F. Yu, M.-H. You, M. Yu, X. Ning, Y.-Z. Long, *J. Phys. Chem. C* **2017**, *121*, 8663.

[14] J. Schneider, P. Rohner, D. Thureja, M. Schmid, P. Galliker, D. Poulikakos, *Adv. Funct. Mater.* **2016**, *26*, 833.

[15] G. Zheng, W. Li, X. Wang, D. Wu, D. Sun, L. Lin, *J. Phys. D: Appl. Phys.* **2010**, *43*, 415501.

[16] J. Deng, C. Liu, M. Madou, *Nanoscale* **2020**, *12*, 10521.

[17] D. George, A. Garcia, Q. Pham, M. R. Perez, J. Deng, M. T. Nguyen, T. Zhou, S. O. Martinez-Chapa, Y. Won, C. Liu, R. C. Lo, R. Ragan, M. Madou, *Microsyst. Nanoeng.* **2020**, *6*, 1.

[18] F. Ruggieri, D. Di Camillo, L. Lozzi, S. Santucci, A. De Marcellis, G. Ferri, L. Giancaterini, C. Cantalini, *Sens. Actuators, B* **2013**, *179*, 107.

[19] Z. Lou, X. Yang, H. Chen, Z. Liang, *J. Semicond.* **2018**, *39*, 024002.

[20] J.-U. Park, M. Hardy, S. J. Kang, K. Barton, K. Adair, D. Kishore Mukhopadhyay, C. Y. Lee, M. S. Strano, A. G. Alleyne, J. G. Georgiadis, P. M. Ferreira, J. A. Rogers, *Nat. Mater.* **2007**, *6*, 782.

[21] Y.-S. Park, J. Kim, J. M. Oh, S. Park, S. Cho, H. Ko, Y.-K. Cho, *Nano Lett.* **2019**, *20*, 441.

[22] G. Luo, K. S. Teh, Y. Liu, X. Zang, Z. Wen, L. Lin, *ACS Appl. Mater. Interfaces* **2015**, *7*, 27765.

[23] G. Zheng, J. Jiang, X. Wang, W. Li, Z. Yu, L. Lin, *Mater. Des.* **2021**, *198*, 109304.

[24] W. E. King, G. L. Bowlin, *Polymers* **2021**, *13*, 1097.

[25] S. Bain, P. Koomsap, D. Parajuli, *Bull. Mater. Sci.* **2021**, *44*, 1.

[26] I. Hayati, A. Bailey, T. F. Tadros, *J. Colloid Interface Sci.* **1987**, *117*, 205.

[27] Z. Sun, J. M. Deitzel, J. Knopf, X. Chen, J. W. Gillespie Jr, *J. Appl. Polym. Sci.* **2012**, *125*, 2585.

[28] L.-G. Liu, J.-H. He, *Therm. Sci.* **2017**, *21*, 1821.

[29] J. T. Jung, J. F. Kim, H. H. Wang, E. Di Nicolo, E. Drioli, Y. M. Lee, *J. Membr. Sci.* **2016**, *514*, 250.

[30] Y. Layec, M.-N. Layec-Raphalen, *J. Phys., Lett.* **1983**, *44*, 121.

[31] K. Nayani, H. Katepalli, C. S. Sharma, A. Sharma, S. Patil, R. Venkataraghavan, *Ind. Eng. Chem. Res.* **2012**, *51*, 1761.

[32] J. Mohr, T. Grund, D. Kunka, J. Kenntner, J. Leuthold, J. Meiser, J. Schulz, M. Walter, *AIP Conf. Proceedings*, Vol. *1466*, American Institute of Physics, College Park, MD **2012**, pp. 41–50.

[33] R. Kessick, G. Tepper, *Appl. Phys. Lett.* **2004**, *84*, 4807.

[34] M. Naeimirad, A. Zadhoush, R. Kotek, R. Esmaeely Neisiany, S. Nouri Khorasani, S. Ramakrishna, *J. Appl. Polym. Sci.* **2018**, *135*, 46265.

[35] R. Khajavi, M. Abbasipour, *Sci. Iran.* **2012**, *19*, 2029.

[36] M. Islam, D. Keck, J. Gilmore, R. Martinez-Duarte, *Micromachines* **2020**, *11*, 255.

[37] S. Forouzanfar, N. Pala, M. Madou, C. Wang, *Biosens. Bioelectron.* **2021**, *180*, 113119.

[38] A. Theron, E. Zussman, A. Yarin, *Nanotechnology* **2001**, *12*, 384.

[39] A. Wexler, *J. Res. Natl. Bur. Stand., Sect. A* **1976**, *80*, 775.

[40] J. Safarov, *Adv. Phys. Res.* **2019**, *1*, 14.

[41] Q. Yang, Z. Li, Y. Hong, Y. Zhao, S. Qiu, C. Wang, Y. Wei, *J. Polym. Sci., Part B: Polym. Phys.* **2004**, *42*, 3721.